Earthquake Engineering & Structural Dynamics
The Journal of the International Association for Earthquake Engineering

EARTHQUAKE ENGINEERING & STRUCTURAL DYNAMICS
Earthquake Engng Struct. Dyn. 2013; **42**:603–622
Published online 17 July 2012 in Wiley Online Library (wileyonlinelibrary.com). DOI: 10.1002/eqe.2232

Near-source seismic hazard and design scenarios

Eugenio Chioccarelli and Iunio Iervolino*,†

Dipartimento di Ingegneria Strutturale, Università degli Studi di Napoli Federico II, Naples, Italy

SUMMARY

Earthquakes damage engineering structures near, relatively to the rupture's size, to the source. In this region, the fault's dynamics affect ground motion propagation differently from site to site, resulting in systematic spatial variability known as directivity. Although a number of researches recommend that records with directivity-related velocity pulses should be explicitly taken into account when defining design seismic action on structures, probabilistic seismic hazard analysis (PSHA), in its standard version, seems inadequate for the scope. In the study, it is critically reviewed why, from the structural engineering point of view, hazard assessment should account for near-source effects (i.e., pulse-like ground motions), and how this can be carried out adjusting PSHA analytically via introduction of specific terms and empirically calibrated models. Disaggregation analysis and design scenarios for near-source PSHA are also formulated. The analytical procedures are then applied to develop examples of hazard estimates for sites close to strike–slip or dip–slip faults and to address differences with respect to the ordinary case, that is, when pulse-like effects are not explicitly accounted for. Significant increase of hazard for selected spectral ordinates is found in all investigated cases; increments depend on the fault-site configuration. Moreover, to address design scenarios for seismic actions on structures, disaggregation results are also discussed, along with limitations of current design spectra to highlight the pulse-like effects of structural interest. Finally, an attempt to overcome these, by means of disaggregation-based scenarios specific for the pulse occurrence case, is presented. Copyright © 2012 John Wiley & Sons, Ltd.

Received 14 October 2011; Revised 14 June 2012; Accepted 15 June 2012

KEY WORDS: forward directivity; PSHA; near-fault; disaggregation; design spectra

1. INTRODUCTION

Most advanced seismic codes worldwide define structural design actions based on probabilistic seismic hazard analysis or PSHA [1, 2], which allows the building of hazard curves starting from seismic source models and ground motion prediction equations (GMPEs). PSHA is, to date, a consolidated procedure; however, the need for adjustments for sites close to a seismic fault, is emerging. In fact, in near-source (NS) conditions, ground motions, and seismic structural response, may show systematic spatial variability PSHA is not able to explicitly capture. This is believed to be due to rupture's directivity, which affects sites in a particular geometrical configuration with respect to the rupture, resulting in velocity fault-normal signals characterized by a large full-cycle pulse at the beginning of the record and containing most of its energy [3]. As an example, in Figure 1 fault normal (FN) and fault parallel (FP) original components of a velocity record from the April 6, 2009 L'Aquila earthquake, the pulse extracted with the algorithm in [4], the residual ground motion after the pulse is removed, and the displacement time histories, are shown. The considered seismic station

*Correspondence to: Iunio Iervolino, Dipartimento di Ingegneria Strutturale, Università degli Studi di Napoli Federico II, via Claudio 21, 80125, Naples, Italy.
†E-mail: iunio.iervolino@unina.it

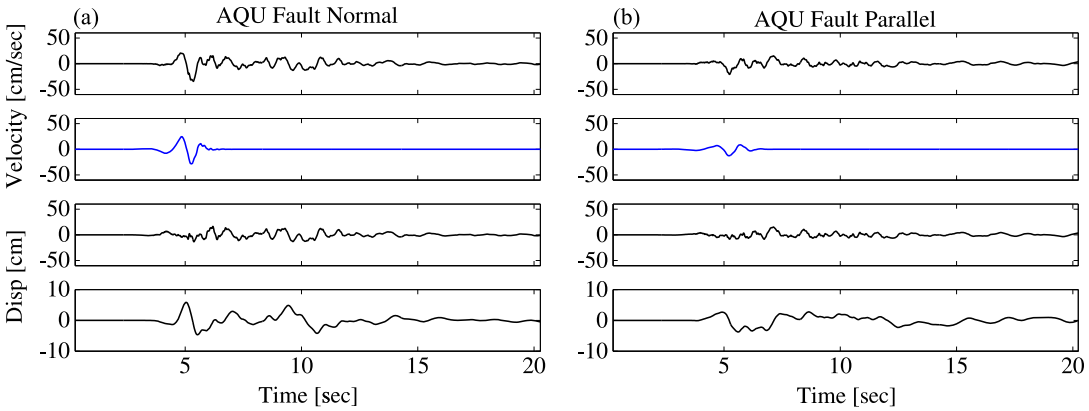

Figure 1. AQU record for the April 6, 2009 L'Aquila earthquake. From top to bottom: velocity time history, extracted pulse, residual velocity, and displacement time history, for (a) FN and (b) FP components.

(AQU[‡]) belongs to the Mediterranean Network (MedNet, http://mednet.rm.ingv.it/) and was less than 10 km far from the epicenter, within the surface projection of the rupture. FN direction, in which directivity effects are usually expected, has been classified as pulse-like with a pulse period (T_p or Tp) equal to 0.99 s. Conversely, FP direction does not show evident pulse-like characteristic. Such results are apparent in Figure 1, if extracted pulses and differences between original and residual time histories are compared.

In a previous study [5] and analyzing a large dataset, three main features of engineering interest characterizing pulse-like records, if compared with those non-pulse-like (hereafter defined as 'ordinary'), were found: (1) pulse-like signals are characterized by FN records generally 'stronger' than FP components (non-pulse-like ground motions have equivalent median FN and FP components); (2) FN pulse-like signals are characterized by a nonstandard spectral shape with an increment of spectral ordinates in a range around T_p; (3) inelastic to elastic seismic spectral displacement ratio for FN pulse-like records may virtually depart from the equal displacement rule, and can be 20%÷70% higher than that of ordinary motions, depending on the nonlinearity level [6]. Such increments are displayed in a range of period between about 30% and 50% of pulse period. A consistent analysis of inelastic displacement demand associated to forward-directivity ground motions is also provided in [7].

Most of the ordinary GMPEs are fitted on ground motion databases in which pulse-like records, if any, are a minority and often rotated differently to FN and FP directions. Moreover, because each record is characterized by a different T_p, the influence of pulse-like spectral shape on such GMPEs is masked and/or spread over a broad range of periods. Finally, GMPEs are somewhat isotropic and do not adequately account for the fault-site position favoring directivity effects. Therefore, it appears pulse-like characteristics to be almost negligible in ordinary GMPEs (see [8] for a discussion). Thus, rupture directivity at near-source sites cannot explicitly appear in classical PSHA.

In the presented study, a review of the literature framework to adjust the hazard analysis in near-source conditions is discussed first, together with all available models for probabilistic assessment of directivity effects with respect to strike–slip (SS) and dip–slip (DS) faults. Classical PSHA and modified (NS-PSHA) are compared, and main differences are pointed out to understand the consequences on hazard assessment. Disaggregation is also formulated explicitly referring to pulse occurrence and pulse absence, and issues in the identification of design scenarios are discussed. To provide a quantitative understanding of the issues involved in NS-PSHA, applications for single seismic sources with strike–slip or dip–slip rupture mechanisms are investigated. Finally, a discussion of possible design spectra in near source conditions is addressed.

[‡]In cases of dip-slip ruptures (e.g., 2009 L'Aquila earthquake), FN and FP are defined as strike-normal and strike-parallel directions respectively. This is consistent with [5], in which several records from L'Aquila earthquake were analyzed for directivity features. AQU record was not available to the authors at the time of the mentioned study.

DOI: 10.1002/eqe

2. NEAR-SOURCE PROBABILISTIC SEISMIC HAZARD ANALYSIS

Recent attempts to explicitly assess directivity effects in probabilistic hazard assessment are aimed at modifying classical PSHA to highlight the pulse-like features of ground motion rather than formulating a new procedure (e.g., [9–11]). This is because PSHA is consolidated, and it is desirable to take advantage of the bulk of tools and knowledge available for it. Moreover, modification enables a relatively easy understanding of the results and analysis of differences. In fact, adjustment of PSHA integrals requires focusing on development of those probabilistic models specific for the NS case, which became available only recently, as the first applications in this field show (i.e., [8, 12]).

Standard approach for computing the mean annual frequency (MAF, λ) of exceeding a ground motion intensity measure (IM) threshold is shown in Equation (1) for a single seismic source. The chosen IM is the elastic spectral acceleration (S_a or Sa) at a fixed spectral period (T^*) exceeding an intensity level, $S_a(T^*) = s_a^*$:

$$\lambda_{S_a}\left(s_a^*\right) = v \cdot \int_m \int_r G_{S_a|M,R}\left(s_a^*|m,r\right) \cdot f_{M,R}(m,r) \cdot \mathrm{d}m \cdot \mathrm{d}r \tag{1}$$

where M is the magnitude and R is the source-to-site distance, v is the mean annual rate of occurrence of earthquakes on the source within a magnitude range of interest, $f_{M,R}$ is the joint probability density function (PDF) of M and R, and $G_{S_a|M,R}$ is the complementary cumulative distribution function (CDF) of S_a (usually lognormal if obtained by a GMPE).

Near-source PSHA requires the MAF to be a linear combination of two hazard terms, which account for the absence or the occurrence of the pulse, $\lambda_{S_a,\mathrm{NoPulse}}$ and $\lambda_{S_a,\mathrm{Pulse}}$ respectively, as reported in Equation (2). In fact, the problem of estimating seismic hazard in near-source conditions may be posed as if two faults are present at the same location: one producing ordinary ground motions, and one producing pulse-like records.

$$\lambda_{S_a}\left(s_a^*\right) = \lambda_{S_a,\mathrm{NoPulse}}\left(s_a^*\right) + \lambda_{S_a,\mathrm{Pulse}}\left(s_a^*\right) \tag{2}$$

The two terms of Equation (2) are implicitly weighted by the pulse occurrence probability. Moreover, two other tasks, which are not faced in traditional hazard analysis, appear: (i) pulse period prediction and (ii) pulse amplitude prediction. In Equations (3) and (4), which expand Equation (2) in the case of a single fault with undefined rupture mechanism, $\underline{Z}$ is a vector with all the required information (to follow) about the relative position between the seismic source and the site (e.g., [10, 11]).

$$\lambda_{S_a,\mathrm{NoPulse}}\left(s_a^*\right) = v \cdot \int_m \int_{\underline{z}} P\left[NoPulse|m,\underline{z}\right] \cdot G_{S_a|M,\underline{Z}}\left(s_a^*|m,\underline{z}\right) \cdot f_{M,\underline{Z}}\left(m,\underline{z}\right) \cdot \mathrm{d}m \cdot \mathrm{d}\underline{z} \tag{3}$$

$$\begin{aligned}\lambda_{S_a,\mathrm{Pulse}}\left(s_a^*\right) = v \cdot \int_m \int_{\underline{z}} \int_{t_p} & P\left[Pulse|m,\underline{z}\right] \cdot G_{S_a,\mathrm{mod}|M,\underline{Z},T_p}\left(s_a^*|m,\underline{z},t_p\right) \cdot f_{T_p|M,\underline{Z}}\left(t_p|m,\underline{z}\right) \\ & \times f_{M,\underline{Z}}\left(m,\underline{z}\right) \cdot \mathrm{d}m \cdot \mathrm{d}\underline{z} \cdot \mathrm{d}t_p\end{aligned} \tag{4}$$

Equation (3) refers to the case of pulse absence and it is weighted for the corresponding probability, $P\left[NoPulse|m,\underline{z}\right]$. All other terms are equal to those of Equation (1) in which pulse-like effects are not considered. Conversely, Equation (4) refers to the case of pulse occurrence as indicated by the pulse occurrence probability, $P\left[Pulse|m,\underline{z}\right]$. To account for the peculiar spectral shape of pulse-like

DOI: 10.1002/eqe

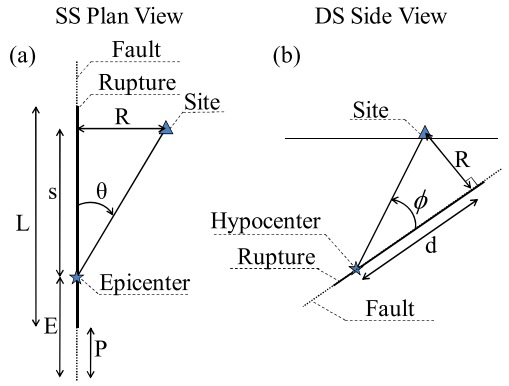

Figure 2. (a) SS and (b) DS geometrical parameters.

records, it is possible to specifically calibrate a new GMPE or to modify an existing one; the latter is considered herein, thus the $G_{S_a,\,\mathrm{mod}|M,\underline{Z},T_\mathrm{p}}$ symbol. Because modification of ordinary GMPEs depends on the pulse period, the $f_{T_\mathrm{p}|M,\underline{Z}}$ distribution is required in the analysis. Finally, $f_{M,\underline{Z}}$ is the joint distribution (of magnitude and geometrical parameters) similar to the ordinary PSHA, but with a more detailed description (by means of $\underline{Z}$) of relative source-to-site position, with respect to the simple distance variable of Equation (1).

The terms appearing in the equations and not shared by classical PSHA, are discussed in the following sections. It will be shown that no significant difficulties are conceptually introduced in the near-source hazard, while computational effort can significantly increase.

2.1. Pulse occurrence probability

The complexity of rupture and wave propagation phenomena makes directivity prediction difficult if based only on physical parameters; in fact it is not always observed in the sites where it is expected, and may also occur at sites apparently not prone to pulse-like ground motion (e.g., [13]). Thus, stochastic models for the prediction of the pulse occurrence probability, $P[Pulse]$, were developed (e.g., [11]). These models depend only on geometrical parameters depicted in Figure 2, which are slightly different in the case of strike–slip or dip–slip faults [3]. Such parameters in SS [DS] case are: (i) distance (s) from the epicenter to the site [d, from hypocenter to the site] measured along the rupture direction, (ii) θ angle between the fault strike and the path from epicenter to the site [ϕ angle between the fault plane and the path from hypocenter to the site], and (iii) minimum distance R between the rupture and the site. (For SS, some additional parameters, which will be addressed in the next sections, are shown in Figure 2.)

Equations (5) and (6) report the two models used in this study; note that the geometrical variables for DS were used in [11] to fit generic non-strike-slip (NSS) data.

$$P[Pulse|R,s,\theta] = \frac{e^{0.859-0.111\cdot R+0.019\cdot s-0.044\cdot\theta}}{1+e^{0.859-0.111\cdot R+0.019\cdot s-0.044\cdot\theta}} \tag{5}$$

$$P[Pulse|R,d,\phi] = \frac{e^{0.553-0.055\cdot R-0.027\cdot d-0.027\cdot\phi}}{1+e^{0.553-0.055\cdot R-0.027\cdot d-0.027\cdot\phi}} \tag{6}$$

Equations (5) and (6) are defined for R (SS), R (DS), s, d, θ or ϕ varying in the intervals[§] of [0 km, 30 km], [5 km, 30 km], [0 km, 40 km], [0 km, 20 km], [0°, 90°], and [0°, 90°], respectively.

[§]In the following examples, zero pulse probabilities are associated to values outside the covariates' intervals where models apply.

DOI: 10.1002/eqe

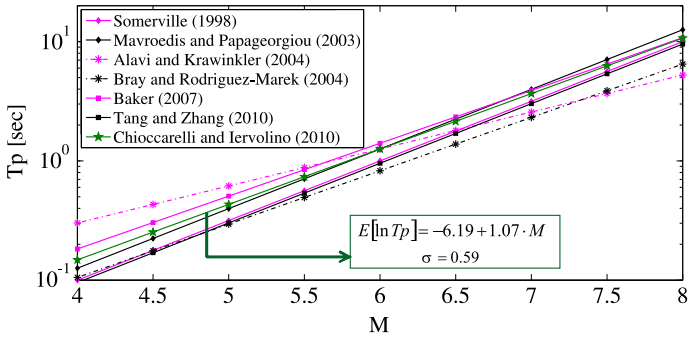

Figure 3. Regression models for T_p.

From the models, it emerges that pulse occurrence probability, even if the site is in the most dangerous position for pulse occurrence, is never equal to one because of the uncertainties associated to forward-directivity effects. SS ruptures are the cases in which effects are easily observed and the highest occurrence probability provided by the model is around 0.8. NSS cases are less prone to directivity effects (likely because of data heterogeneity) and the highest computed probability is around 0.4. In both cases, occurrence probability decreases rapidly with increasing distance and decreasing *s*-parameter [*d*-parameter].

2.2. *Pulse period*

Somerville [14] suggests that pulse period is related to source parameters such as the rise time (duration of slip on the fault) and fault dimensions, which generally increase with *M*. Other authors (e.g., [4, 5, 13, 15–20]) analyzed pulse period dependency and produced models for the evaluation of T_p as summarized in [18]. A linear relationship between moment magnitude and the logarithm of T_p is adopted by all of them, following the indication in [14]; Figure 3. Comparing models, differences may be found, but it is worth noting that there is no consistency in procedures to identify pulse periods and datasets among the different studies. Standard deviations of the residuals, not reported here for all cases, are always large, likely for the influence of other perturbations such as site or propagation. The regression in [5], is used in the following applications. Developing such a regression, T_p was found, in fact, to be significantly dependent only on *M* if compared with the other variables in Equation (4); others (e.g., [13, 19, 20]) found a minor dependency on *R* and soil properties, even if in some cases only.

2.3. *Ground motion prediction equation*

To have a suitable GMPE in the case of pulse occurrence, the modifying factor suggested in [21] is applied to an already existing prediction equation. The semi-empirically calibrated factor refers to the natural logarithm of the predicted[¶] spectral acceleration as shown in Equation (7), and it models the systematic deviation of elastic spectral shapes of FN pulse-like signals with respect to ordinary.

$$\overline{\ln(S_a(T))} = \ln(S_a(T)) + e^{-\left(\ln\left(T/T_p\right)\right)^2} \tag{7}$$

In the equation $\ln(S_a(T))$ is the original GMPE, $\overline{\ln(S_a(T))}$ is the logarithm of the predicted acceleration via the modified GMPE, and $e^{-\left(\ln\left(T/T_p\right)\right)^2}$ models the 'bump' of spectral ordinates with a maximum at $T = T_p$.

[¶]This modification only affects the prediction of the mean of the logarithms, while standard deviation may also potentially change. Because treatment of standard deviation has, in general, relevant effects on hazard analysis, the interested reader is referred to [8] for a discussion about GMPE standard deviation modification in NS conditions.

DOI: 10.1002/eqe

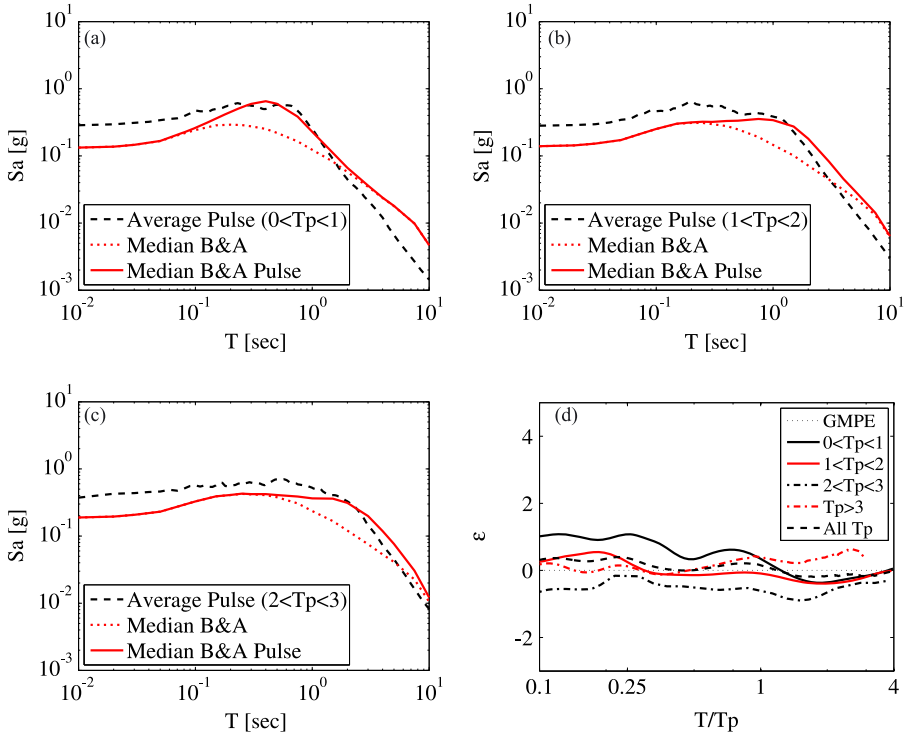

Figure 4. Application of amplification factor for pulse-like records grouped for T_p between (a) 0 and 1.0 s, (b) 1.0 and 2.0 s, (c) 2.0 and 3.0 s, and (d) ε computed using the modified GMPE.

To understand the effectiveness and limitations of this modification, a set of 73 pulse-like records (34 SS and 39 NSS) taken from the Next Generation Attenuation (NGA) database (http://peer.berkeley.edu/nga/) was analyzed. Pulse-like records are grouped in bins of T_p and average spectra of each group are reported in Figures 4(a), (b), and (c) (indicated as Average Pulse). In the same figures, for each record, expected median spectra have been computed with the GMPE in [22], and the average of such spectra is reported (Median B&A). Average median spectra have been computed also from the modified GMPE (Median B&A Pulse). Figures show that, while the modified GMPE approximates[‖] the pulse-like spectral shape, it also seems that the portion of the spectrum affected by the bump is large, although directivity effects are commonly referred to as narrow band, to distinguish from period-independent, or broad-band, GMPE modifications (e.g., [3]).

It is also worth noting a significant difference between the average recorded spectra and the medians, predicted by both GMPEs, in high frequency ranges. It may suggest that directivity effects also influence low structural periods (as discussed in Section 1) even if the modification factor does not account for such an influence (e.g., [5]).

Figure 4(d) shows, for the same groups of NGA records, the number of standard deviations by which the logarithmic ground motion departs from the median predicted by the modified GMPE (ε). Average values for each T_p bin are reported as a function of T/T_p. As discussed, it appears that the modified GMPE works better in the low frequency range (comparatively to T_p) with respect to the high frequency; however, the modification factor can be considered generally helpful in modeling pulse-like effects.

3. SPECIFIC RUPTURES

After a description of the peculiar models required by NS-PSHA, Equations (3) and (4) can be analyzed in more detail. Such a deepening, which does not change the described framework from

[‖]Modification factor of [21] has been fitted on a slightly different set of records, while it refers to the same GMPE.

DOI: 10.1002/eqe

literature (i.e., [10]), results in a transformation of variables required for the numerical implementation of near-source hazard in SS and DS cases. In fact, being the pulse occurrence probability model a function of geometrical parameters, for each application it is required to know the rupture and epicenter or hypocenter in SS and DS cases, respectively. (Finally, it is worth noting that the following focuses on introduction of pulse-like characteristics in PSHA, other issues common to ordinary PSHA, such as epistemic uncertainty, are determinedly left out because they are widely analyzed in existing literature, for example, Ref. [2].)

3.1. Strike–slip

In the case of an individual SS source of fixed dimensions and geographical location, the necessary geometrical parameters to compute hazard are the rupture length (L, assumed to be lower or equal to the fault length), the position of the rupture on the fault (P), and the epicenter location (E) as reported in Figure 2(a). A deterministic relationship between these parameters and $\{R,s,\theta\}$ vector exists. Thus, the $\underline{Z}$-vector in Equations (3) and (4) can be replaced by a vector comprised of L, P, and E.

In the analysis, L can be considered as a function of magnitude (e.g., [23]), while P and E may be associated to a uniform probability distribution on the fault (constrained to not exceed fault boundaries) and on the rupture length, respectively. Given these assumptions, Equations (3) and (4) are specialized for the SS particular case, obtaining Equations (8) and (9).

$$\lambda_{S_a,NoPulse}\left(s_a^*\right) = \nu \cdot \int_m \int_l \int_p \int_e P[NoPulse|m,l,p,e]\cdot G_{S_a|M,L,P,E}\left(s_a^*|m,l,p,e\right) \times f_{P,E|M,L}(p,e|m,l)\cdot f_{L|M}(l|m)\cdot f_M(m)\cdot \mathrm{d}m\cdot \mathrm{d}l\cdot \mathrm{d}p\cdot \mathrm{d}e \tag{8}$$

$$\lambda_{S_a,Pulse}\left(s_a^*\right) = \nu \cdot \int_{t_p} \int_m \int_l \int_p \int_e P\left[Pulse|t_p,m,l,p,e\right]\cdot G_{S_a,\,\mathrm{mod}|T_p,M,L,P,E}\left(s_a^*|t_p,m,l,p,e\right) \times f_{T_p|M,L,P,E}\left(t_p|m,l,p,e\right)\cdot f_{P,E|M,L}(p,e|m,l)\cdot f_{L|M}(l|m)\cdot f_M(m)\cdot \mathrm{d}t_p\cdot \mathrm{d}m\cdot \mathrm{d}l\cdot \mathrm{d}p\cdot \mathrm{d}e \tag{9}$$

It appears that to account for all the geometrical parameters, a fifth-order integral is necessary, leading to a computational effort significantly higher than ordinary PSHA.[**] In fact, Equations (8) and (9) can be simplified neglecting some stochastic dependencies. More specifically:

- Pulse probability is a function of geometrical parameters and is independent on magnitude and pulse period, that is, $P[Pulse|t_p,m,l,p,e] = P[Pulse|l,p,e]$;
- Pulse period PDF is a function of magnitude only, that is, $f_{T_p|M,L,P,E}\left(t_p|m,l,p,e\right) = f_{T_p|M}\left(t_p|m\right)$;
- PDF of rupture and epicenter's position depends on the rupture length, that is, $f_{P,E|M,L}(p,e|m,l) = f_{P,E|L}(p,e|l)$;
- $G_{S_a,\,\mathrm{mod}|T_p,M,L,P,E}$ is the modified GMPE, and $G_{S_a|M,L,P,E}$ is the original GMPE. Using R_{jb}, both functions are independent on the location of the epicenter, E;
- Pulse occurrence and absence are complementary: $P[NoPulse|l,p,e] = 1 - P[Pulse|l,p,e]$.

3.2. Dip–slip

Pulse occurrence probability model considers DS in its two-dimensional representation, which is easy to render analogous to the SS case[††] (Figure 2). In fact, dip–slip three-dimensional representation is given in Figure 5 by two orthogonal sections, which may be useful to identify all the geometrical variables needed, and those that can be neglected in the hazard integrals.

[**] If in ordinary PSHA epicentral distance is used, two geometrical variables (L and P) may be not explicitly considered; if R_{jb} (i.e., [24]) distance metric is used, E variable can be neglected. Finally, ordinary PSHA is independent of T_p.

[††] In principle, also SS ruptures are worth of a three-dimensional representation.

DOI: 10.1002/eqe

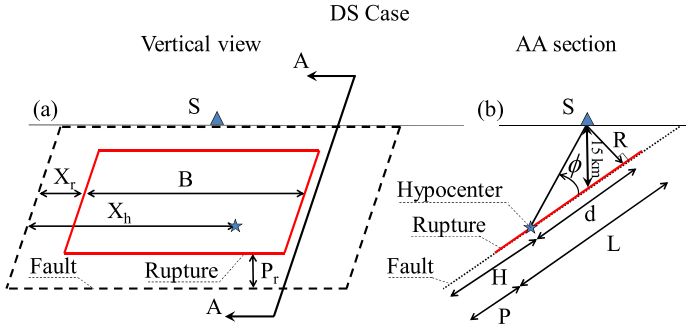

Figure 5. Dip–slip rupture representation (some symbols will be recalled in the applications' section).

For simplicity, the hypotheses of rectangular fault and rupture are taken here. B and L variables represent rupture surface sides (Figures 5(a) and (b)). As for SS, they can be computed using [23], which provide relationships as functions of M for each of the two linear dimensions and the total rupture area. A possible option (used in the following applications) is to assume only one of the three mentioned parameters as a variable (dependent on event magnitude) and forcing a constant ratio for B and L.

X_r and X_h are the distances of the rupture and of the hypocenter from the fault bounds, respectively. The former is necessary for the identification of R_{jb} of the site for which hazard is computed, and it has to appear in the hazard integral, while the latter can be neglected. In fact, the hypocenter's position is important for parameters represented by section AA in Figure 5, where X_h does not appear.

Equations (8) and (9) can be adapted to the dip–slip case, that is, Equations (10) and (11), considering the following differences (simplifications discussed in the previous section hold):

(1) Position of the epicenter, E, has to be replaced by the position of the hypocenter (H);
(2) The rupture's geometrical parameter dependent on event magnitude is assumed to be the rupture length L, in analogy with the SS case (in principle it should be the area of the rupture from which B and L are assumed to be deterministically dependent in the hypothesis of a constant B/L ratio);
(3) To compute pulse occurrence probability X_r is also necessary (for computation of R, along L, P, and H);
(4) The introduction of X_r requires knowledge of its PDF conditional to L, $f_{X_r|L}(x_r|l)$. Such distribution is, in principle, also conditional on the dimension and position of the fault; however, they are considered as known.

$$\lambda_{S_a,NoPulse}\left(s_a^*\right) = \nu \cdot \int_m \int_l \int_p \int_h \int_{x_r} P[NoPulse|l,p,h,x_r] \cdot G_{S_a|M,X_r,L,P}\left(s_a^*|m,l,p,x_r\right) \times f_{P,H|L}(p,h|l) \cdot f_{X_r|L}(x_r|l) \cdot f_{L|M}(l|m) \cdot f_M(m) \cdot \mathrm{d}m \cdot \mathrm{d}l \cdot \mathrm{d}p \cdot \mathrm{d}h \cdot \mathrm{d}x_r \quad (10)$$

$$\lambda_{S_a,Pulse}\left(s_a^*\right) = \nu \cdot \int_{t_p} \int_m \int_l \int_p \int_h \int_{x_r} P[Pulse|l,p,h,x_r] \cdot G_{S_a,\,\mathrm{mod}|T_p,M,X_r,L,P}\left(s_a^*|t_p,m,l,p,x_r\right) \times f_{T_p|M}\left(t_p|m\right) \cdot f_{P,H|L}(p,h|l) \cdot f_{X_r|L}(x_r|l) \cdot f_{L|M}(l|m) \cdot f_M(m) \cdot \mathrm{d}t_p \cdot \mathrm{d}m \cdot \mathrm{d}l \cdot \mathrm{d}p \cdot \mathrm{d}h \cdot \mathrm{d}x_r \quad (11)$$

It is noted that, in the DS case, integration becomes as large as over six variables, if the simplified hypothesis of constant B/L ratio is retained (otherwise, one more variable should be considered, being that the rupture is a two-dimensional phenomenon).

DOI: 10.1002/eqe

4. APPLICATIONS

Because the marginal pulse occurrence probability is generally fairly low according to [11], applications of the proposed approach are required to assess quantitatively the effects of these modifications on seismic hazard estimates, and whether NS-PSHA is able to represent the pulse-like directivity threat adequately (i.e., worth with respect to the enlarged analytical effort required). To this aim, some applications are developed in terms of hazard (Sections 4.1 and 4.2), disaggregation (Section 5.1), and definition of design spectra (Section 6.3). The geometrical configuration of the examples is analyzed in detail in the following, yet there are some common assumptions and working hypotheses that may be anticipated:

(1) Because modification factor of GMPE accounting for pulse-like effects was fitted on the model in [22], this GMPE is used;
(2) Chosen IMs are the elastic spectral accelerations at all the spectral periods provided by used GMPE (from 0 s, that is, peak ground acceleration or PGA, to 10 s); thus, results are first represented in terms of elastic response spectrum characterized by the same exceedance probability in a fixed time window for all ordinates (i.e., the uniform hazard spectrum, UHS);
(3) A return period (T_r) equal to 475 years is assumed: in other words, computed intensity measures have an exceedance probability in 50 years equal to 10% (assuming a homogeneous Poisson process for earthquake occurrence [1, 2]);
(4) The annual rate of earthquake occurrence (ν) on each fault is assumed to be equal to 0.05.

4.1. Application 1

In this section an SS fault and two different construction sites are considered: site S_1 is aligned with fault direction and located 5 km far from its upper edge, while site S_2 is on the center of the fault (Figure 8(a)). Both sites are expected to be prone to directivity, having a θ angle equal to zero (e.g., [3, 11]). Fault length is assumed equal to 200 km while rupture length (L) and rupture location on the fault (P) are considered as random variables. The distribution of the former, conditional to M, is lognormal[‡‡] (e.g., [23]), while that of the latter is uniform and limited by the fault dimension and the rupture length itself. In fact, for a given size, the rupture can be located in all the possible positions with a uniform probability distribution constrained by the fault limits. R_{jb} of the site is univocally defined once the rupture position is known. Also, the epicenter can ideally be located at any point within the rupture, but to reduce the numerical effort of the illustrative analyses, only three possible positions of the epicenter were considered, that is, in the middle of the rupture or located at 30% of the total rupture length, measured from each of the two rupture extremities. Once the epicenter location is defined, s-parameter is known.

The algorithm implemented for numerical solution of Equations (8) and (9) is shown by the flow chart in Figure 6: for a fixed value of spectral period and s_a^* threshold, it consists of five iterative cycles over the five stochastic variables of the problem $\{t_p, m, l, p, e\}$.

As a first case, the assumption that all the earthquakes generated by the source have a fixed (characteristic) magnitude equal to 7, was considered, and analyses were performed for both sites. Then, referring only to S_1, a Gutenberg–Richter-like distribution [25] for M was assumed with a negative slope equal to -1, and minimum and maximum M equal to 4.5 and 7.5, respectively. To reduce the computational effort, magnitude distribution was lumped by three discrete values[§§] of 5, 6, and 7; the corresponding associated discrete probabilities are respectively 0.9, 0.09, and 0.01 (Figure 8(b)).

Before discussing results, it may be useful to plot PDFs of pulse period and rupture length conditional on those magnitudes considered. Figure 7(a) shows that, if generated earthquakes have M equal to five, it is very unlikely that forward directivity effects affect spectral periods higher than 3 s, while an M 7 earthquake may influence a very large range of structural periods. This is because,

[‡‡]Rigorously, fault length is a physical upper limit for rupture length PDF, but chosen fault dimension (200 km) does not have any practical influence on rupture length distributions for all the cases addressed here.
[§§]Sensitivity analysis, not reported here for sake of brevity, was carried out in order to verify that less coarse discretizations of epicentral location and magnitude distribution (in the Gutenberg–Richter case) do not significantly affect the results presented in the next section.

DOI: 10.1002/eqe

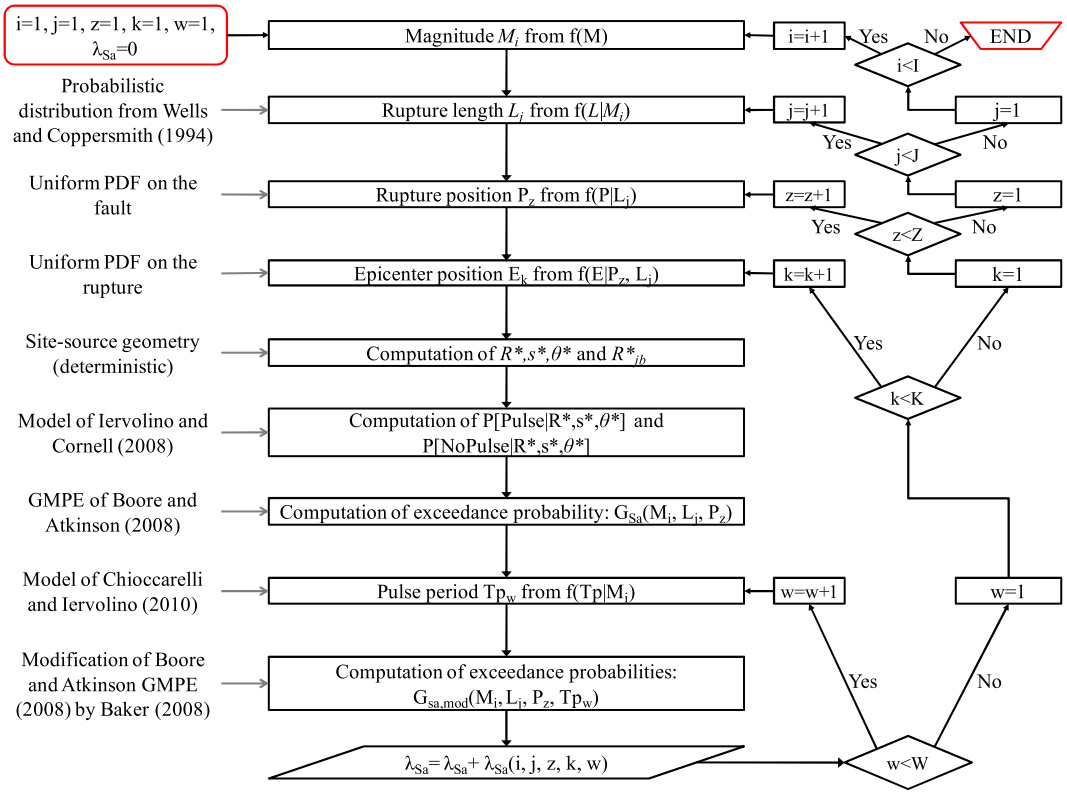

Figure 6. Flow chart of hazard analysis in SS case (capital indices are iteration limits).

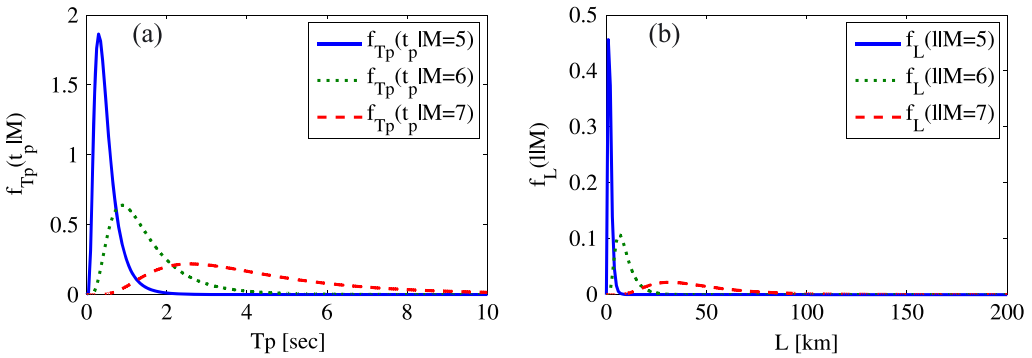

Figure 7. (a) Probability density function of T_p and (b) rupture length L conditional to M equal to 5, 6, and 7.

according to the considered model, standard deviation of the logarithms is 0.59, which means about 60% coefficient of variation of T_p. Moreover, an M 5 earthquake has an associated rupture length significantly lower than the total length of the considered fault (Figure 7(b)), thus its probability of being located near the considered sites is lower than that associated to an M 7 event.

Results of NS-PSHA were compared with the corresponding ordinary hazard estimates; that is, Equation (1). In Figure 8(c), UHS are reported for ordinary ($S_{a_{PSHA}}$) and modified ($S_{a_{NS-PSHA}}$) analyses, and for characteristic and multiple M cases (magnitude distribution is applied only for S_1 and hereafter results for S_2, with characteristic magnitude, will be indicated with a cross superscript: $S_{a_{PSHA}}^{+}$ and $S_{a_{NS-PSHA}}^{+}$). In Figure 8(d) the increments because of forward directivity effects, with respect to the ordinary case, are reported for each case.

Figure 8(c) shows that three analyzed cases yield different results: referring to PGA (for which directivity effects are negligible according to the assumed framework), it is apparent and expected that

DOI: 10.1002/eqe

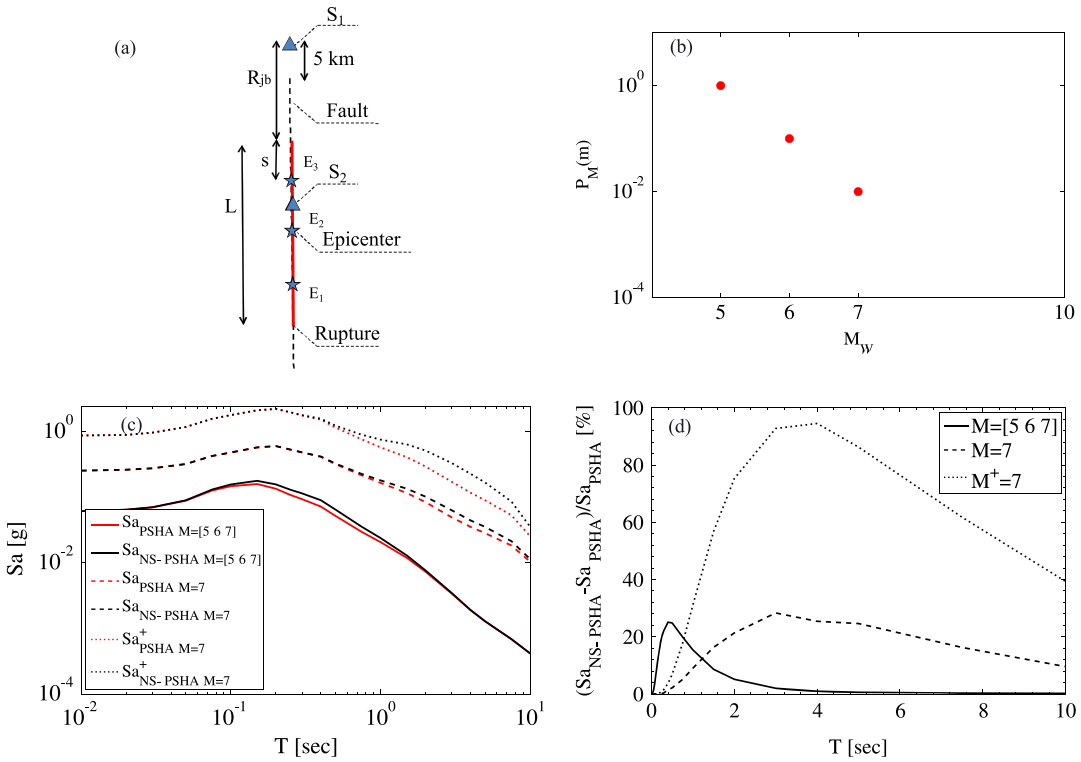

Figure 8. (a) Rupture-site configuration of analyzed cases; (b) mass probability distribution of magnitude occurrence; (c) 475-year UHS; and (d) hazard increments.

characteristic earthquakes generate higher accelerations for S_2 because of the lower distance from the rupture. The lower response spectrum for S_1, in the case of multiple-magnitude distribution, with respect to the case of characteristic magnitude, is of less intuitive understanding, but can be explained recalling that frequency of occurrence of M 5 is much higher than those of M 6 and M 7 (see Figure 8(b)).

Because of the aim of the study and working hypotheses, more attention is given to hazard increments with respect to the ordinary case, rather than on absolute acceleration values, and from Figure 8(d) the following may be pointed out.

(1) Hazard increments vary from about 25% to about 100% depending on the characteristics of the investigated case. This is mainly because of the applicability range of pulse occurrence probability model (see Section 2.1). For site S_1, a zero pulse probability is associated to a number of rupture's positions larger than S_2 (directivity effects are likely to occur more frequently for S_2 rather than for S_1 site). It can also be inferred that, under the hypotheses of uniform distribution of rupture position on the fault, geometry and magnitude occurrence may have significant effects on increments values. In fact, a similar quantitative application is provided in [8] assuming a different geometrical configuration and a different magnitude occurrence model. In that case, amplification of hazard at 5 s spectral acceleration was found equal to 40% for a site subjected to a SS fault and located on the fault.

(2) The shape of hazard increments, the range of spectral periods in which increments are significant, and the period corresponding to the maximum directivity effect, can be directly derived from the model of magnitude occurrence on the fault. Such a dependency derives from the pulse period prediction model; e.g., the PDF of T_p conditional to M 7, has a median value equal to 3.7 s, which is a good approximation of the period corresponding to maximum increment in Figure 8(d).

(3) Similarly, because cases with multiple magnitudes are mostly affected by smaller and more frequent events, the period of maximum increments for the multiple-magnitude distribution is well correlated with the median value of T_p distribution for M 5 (0.43 s), while increments are negligible for spectral periods higher than 4 s.

DOI: 10.1002/eqe

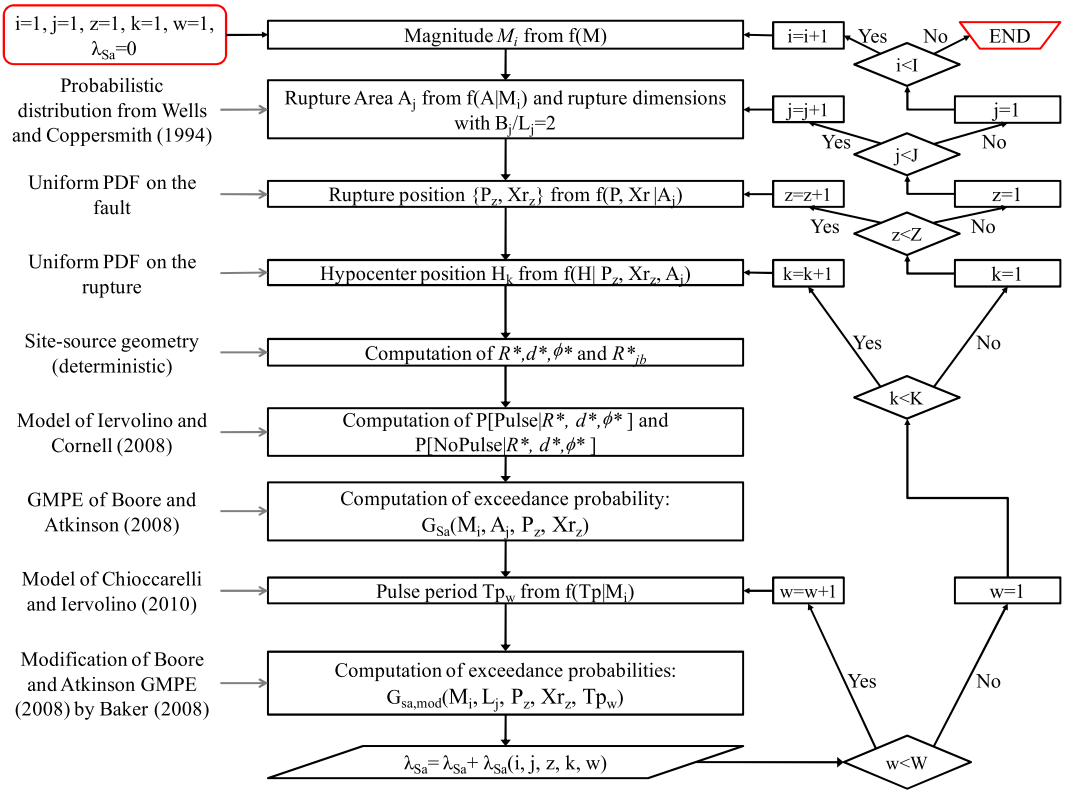

Figure 9. Flow chart of hazard analysis in DS condition (capital indices are iteration limits).

4.2. *Application 2*

In this example, a DS rupture is considered and, similar to the SS examples, fixed planar dimensions (4000 km^2) and position are assumed for the seismic source. In fact, the fault is identified by the following angles: 50° and 90° for dip and rake, respectively; that is, a normal fault. Both fault and rupture areas are assumed to be rectangular with the *B*/*L* ratio equal to two. An individual possible event magnitude, M 7, is assumed.

A site (S) placed within the surface projection of the rupture is considered and reported in Figure 5. In the same figure, size and position of the fault are represented by dotted lines. The rupture's area (A) (or its sides B and L) and location (identified by distance to fault sides, X_r and P_r), are random variables. A-area is assumed to be a lognormally distributed conditional to M [23], and it is limited by the fault dimensions. For a given A-value,[¶¶] the rupture can be located in all the possible positions with a uniform PDF, yet constrained by the fault boundaries. R_{jb} for the site is univocally defined once the rupture is known. Ideally, the hypocenter can also be located everywhere on the rupture, but to reduce the computational demand, only three possible positions on the diagonal of the rupture were assumed. In Figure 5, the generic position of the hypocenters is identified as H. Once the hypocenter is also known, the d-parameter can be determined.

Hazard integral in case of dip–slip ruptures is reported in Equations (10) and (11). The corresponding flow chart is shown in Figure 9. UHS computed with ordinary and modified PSHA are reported in Figure 10(a), while increments are shown in Figure 10(b). The shape of hazard increments is analogous to SS, because it depends only on distribution of T_p given magnitude, which is the same in the two cases. Conversely, values of such increments are different because of the different geometrical configuration.

[¶¶]Similar to the SS case, fixed size of the seismic source does not affect significantly the PDF of rupture size.

DOI: 10.1002/eqe

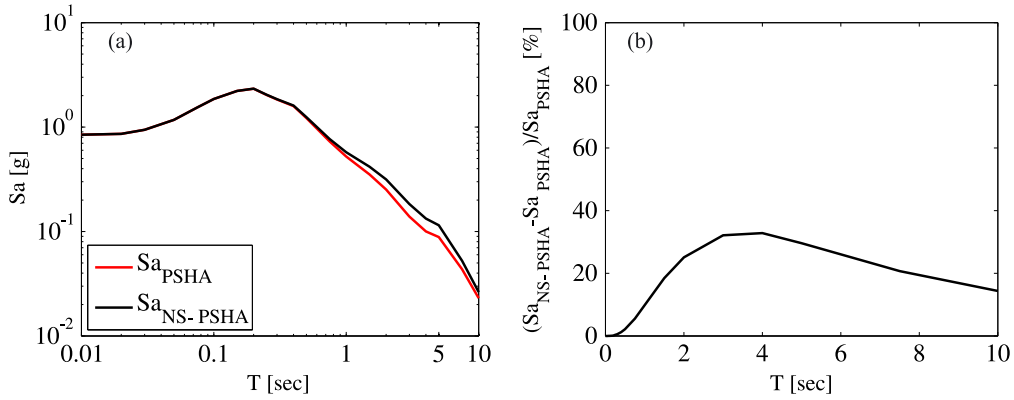

Figure 10. (a) 475-year UHS with modified and classical PSHA and (b) increments because of directivity effects.

5. PULSE-LIKE DISAGGREGATION

Disaggregation is complementary to hazard analysis [26, 27], and it is useful to identify probability-based design scenarios (e.g., design earthquakes [28]) and to provide a rational basis for the selection of representative seismic input (e.g., ground motions) to be used in dynamic analyses of structures. In fact, it is typically used to compute the distribution of magnitudes, distances, and ε values contributing to occurrence or exceedance of some ground motion intensity level $\left(s_{\mathrm{a}}^{*}\right)$. This issue is especially important in near-source conditions in which criteria for design scenarios and ground motion record selection criteria are not well established yet. In fact, classical disaggregation equations can be modified in accordance with the expressions of NS-PSHA, to provide contribution to hazard of the main variables; that is, the probability that a ground motion intensity level is caused by a pulse-like ground motion, and the distribution of pulse periods associated to it, or the probability that a set of geometrical parameters determines the exceedance of a hazard threshold.

Referring to the hypotheses of a single fault, and comprising site-source geometrical parameters with the $\underline{Z}$ vector, disaggregation's most synthetic result is

$$f\left(m,\underline{z},\varepsilon|S_{\mathrm{a}}>s_{\mathrm{a}}^{*}\right)=\frac{v\cdot P\left[S_{\mathrm{a}}>s_{\mathrm{a}}^{*}|m,\underline{z},\varepsilon\right]\cdot f\left(m,\underline{z},\varepsilon\right)}{\lambda_{s_{\mathrm{a}}^{*}}} \tag{12}$$

in which $P\left[S_{\mathrm{a}}>s_{\mathrm{a}}^{*}|m,\underline{z},\varepsilon\right]$ is the probability of exceeding the hazard level s_{a}^{*} given magnitude, ε and all the geometrical variables of the problem. Applying the total probability theorem referring to pulse and no pulse occurrence, Equation (12) becomes

$$f\left(m,\underline{z},\varepsilon|S_{\mathrm{a}}>s_{\mathrm{a}}^{*}\right)=\frac{v\cdot P\left[S_{\mathrm{a}}>s_{\mathrm{a}}^{*}|Pulse,m,\underline{z},\varepsilon\right]\cdot P\left(Pulse|m,\underline{z},\varepsilon\right)\cdot f\left(m,\underline{z},\varepsilon\right)}{\lambda_{s_{a}^{*}}}+ \tag{13}$$

$$+\frac{v\cdot I\left[S_{\mathrm{a}}>s_{\mathrm{a}}^{*}|NoPulse,m,\underline{z},\varepsilon\right]\cdot P\left(NoPulse|m,\underline{z},\varepsilon\right)\cdot f\left(m,\underline{z},\varepsilon\right)}{\lambda_{s_{a}^{*}}}$$

in which I is an indicator function that equals 1 if S_{a} is larger than s_{a}^{*} and zero otherwise. Equation (13) means that, given the S_{a} threshold (i.e., the intensity for which hazard is disaggregated, s_{a}^{*}), disaggregation results is a joint probability function of several variables and it can be obtained performing two disaggregation analyses in the hypothesis of pulse occurrence and pulse absence, respectively. In fact,

DOI: 10.1002/eqe

as discussed when introducing NS-PSHA, this may be seen as if the fault is split into two sources: one determining only pulse-like ground motions and one producing an earthquake with ordinary records.

Also note that in the first term at the right-hand side of Equation (13), the indicator function, I, does not appear because, when conditional to the pulse occurrence and to a defined set of magnitude, ε and geometrical parameters, exceedance of hazard threshold s_a^* is not deterministic, that is, still dependent on T_p.

Marginal disaggregation distribution of pulse period can also be obtained considering only the case of pulse occurrence as reported in Equation (14)

$$f\left(t_p|S_a > s_a^*, Pulse\right) = \frac{\nu \cdot P\left[S_a > s_a^*|t_p, Pulse\right] \cdot f\left(t_p|Pulse\right)}{\lambda_{s_a^*|Pulse}} \tag{14}$$

where $\lambda_{s_a^*|Pulse}$ is the MAF of exceeding the s_a^* value given that the pulse occurs, while $\lambda_{s_a^*,Pulse}$ of Equation (2) is the MAF of the joint event of exceeding s_a^* and occurrence of pulse.

As a final result, probabilities of observing pulse occurrence or absence given the exceedance of s_a^* can be computed. They give information about how likely exceedance is due to forward directivity effects. The two terms are mutually exclusive and complementary to one; analytical expression of the former is reported in Equation (15).

$$P\left[Pulse|S_a > s_a^*\right] = \frac{\nu \cdot P\left[S_a > s_a^*|Pulse\right] \cdot P[Pulse]}{\lambda_{s_a^*}} \tag{15}$$

In the following section, the discussion about disaggregation is expanded in near-source conditions, based on the applications developed in Section 4.1. Although they refer to SS, conclusions can be generalized.

5.1. Causative earthquakes for Application 1

Referring to the hazard result of the SS case with a multiple-magnitude distribution (Section 4.1), the disaggregation distributions in Equations (16) and (17) were computed for S_a (1 s):

$$f\left(m, r, \varepsilon, t_p|S_a > s_a^*, Pulse\right) = \frac{\nu \cdot P\left[S_a > s_a^*|Pulse, m, r, \varepsilon, t_p\right] \cdot f\left(m, r, \varepsilon, t_p|Pulse\right)}{\lambda_{s_a^*|Pulse}} \tag{16}$$

$$f\left(m, r, \varepsilon|S_a > s_a^*, NoPulse\right) = \frac{\nu \cdot P\left[S_a > s_a^*|NoPulse, m, r, \varepsilon\right] \cdot f(m, r, \varepsilon|NoPulse)}{\lambda_{s_a^*|NoPulse}} \tag{17}$$

where $f\left(m, r, \varepsilon, t_p|S_a > s_a^*, Pulse\right)$ is the probability of $\{m, r, \varepsilon, t_p\}$ being the causative vector for s_a^* in the case of pulse occurrence, and $f\left(m, r, \varepsilon|S_a > s_a^*, NoPulse\right)$ is the probability of $\{m, r, \varepsilon\}$ being the causative vector in the case of no pulse occurrence in ground motion.

Because some of the considered PDFs cannot be clearly represented (being defined in spaces of order larger than $\Re^3$) numerical integration was used to obtain marginal distribution of easier graphical handling; for example, Equation (18).

$$f\left(m, r|S_a > s_a^*, Pulse\right) = \int_{t_p} \int_{\varepsilon} f\left(m, r, \varepsilon, t_p|S_a > s_a^*, Pulse\right) \cdot d\varepsilon \cdot dt_p \tag{18}$$

In Figure 11 the following disaggregation PDFs are reported: magnitude and distance conditional to pulse (a), and no-pulse (b) occurrence; ε values conditional to pulse (c), and no-pulse (d) occurrence; pulse period in case of pulse (e). All PDFs refer to $T_r = 475$ years.

DOI: 10.1002/eqe

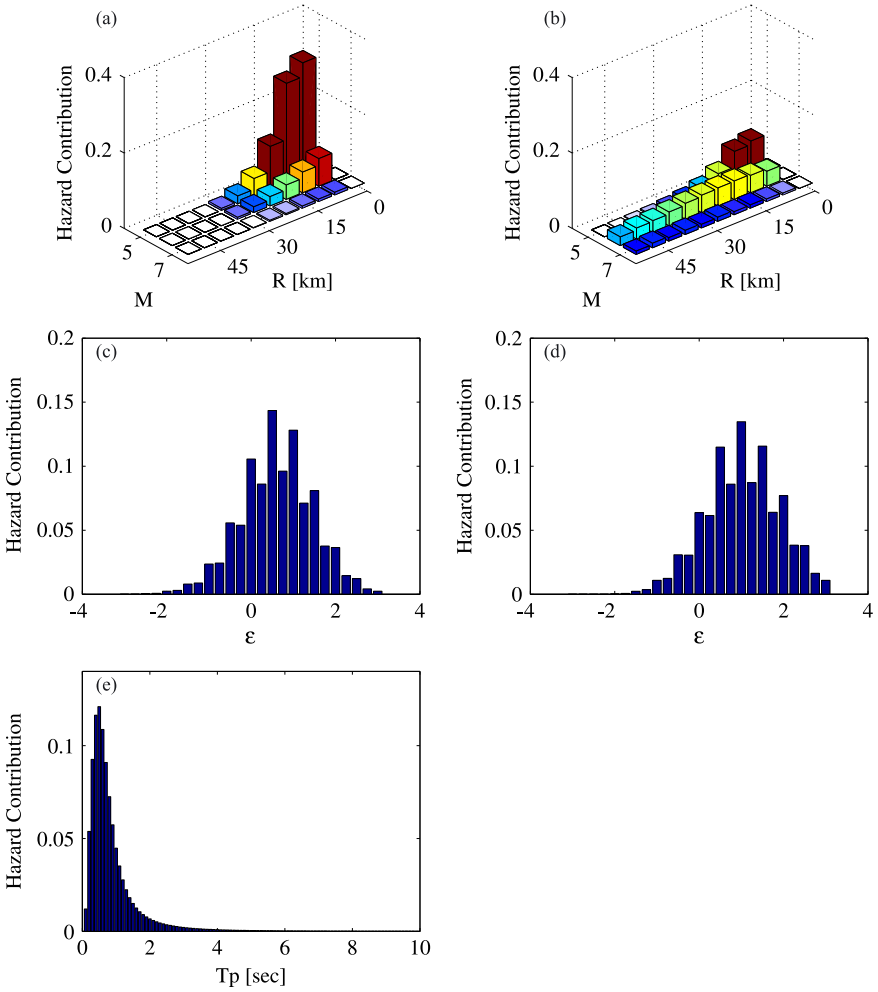

Figure 11. Hazard disaggregation, for $T_r = 475$ years and 1 s spectral period, in terms of: magnitude and distance conditional to (a) pulse occurrence and (b) pulse absence; ε values conditional to (c) pulse occurrence and (d) absence; (e) pulse period.

Distance disaggregation, conditional to pulse occurrence, is limited by the definition domain of the pulse probability model (see Section 2.1). Conversely, the same disaggregation plot, but conditional to absence of pulse, shows non-negligible hazard contributions for larger distances (however, data for distances larger than 50 km are not reported).

Mean ε, conditional to pulse occurrence, is lower than ε conditional to pulse absence (0.5 and 1.0, respectively), because the first disaggregation is computed by the modified GMPE in which T_p effects are applied on the predicted median by the modification factor of Equation (7). Finally, the T_p disaggregation distribution has a similar shape of the PDF of T_p conditional to M 5 (Figure 7(a)); however, because disaggregating hazard refers to 1 s spectral acceleration, the mean is moved from 0.5 to 0.9 s.

6. DESIGN SCENARIOS

It is well known that the uniform hazard spectrum (UHS) does not account for correlation of spectral ordinates. In fact, UHS is an envelope spectrum, which may not be representative of any specific ground motion. The problem was studied for ordinary conditions by Baker and Cornell [29]. The

DOI: 10.1002/eqe

proposed solution consists of the conditional-mean spectrum considering ε (CMS-ε); that is, a spectrum in which the spectral ordinate associated to the structural period of interest has a defined exceedance probability and all the others are computed from disaggregation for the considered structural period, and account for correlation.

In NS-PSHA, resulting UHS is the envelope of many seismic scenarios in which cases of pulse occurrence are combined with cases of pulse absence weighted by the pulse probabilities. Moreover, terms characterized by pulse occurrence account for many different pulse periods, having the PDF of T_p, conditional on event magnitude, a quite flat shape (see Figure 7(a)). As a consequence, the effect of pulses on the final spectrum is spread over a large range of periods as shown in the previous examples. Thus, the well-known limitations of UHS may be even worse in NS cases. On the other hand, CMS-ε is not of easy direct application in the NS-PSHA framework because, to date, an assessment of correlation of spectral ordinates fitted on pulse-like records is not yet available (if not indirectly via the GMPE modification factor), and because it is not univocally defined how to account for T_p in the CMS-ε procedure.

Here, a procedure for identification of design spectra is preliminarily proposed. It consists of the identification of two different spectra representative of the ordinary scenario (i.e., in which no forward directivity effects occur) and the pulse-like scenario (i.e., which accounts entirely for the effects of forward directivity). The latter will be referred to as close-impulsive spectrum or CIS.

6.1. Pulse-like scenario

Proposed procedure for computing CIS can be summarized in the following steps.

(1) Computing average values (or other statistics) of M and R disaggregation distribution in the pulse case; namely, $\{M_{p,\mu}, R_{p,\mu}\}$.
(2) Computing the mean value of pulse period, T_{p_μ}, from its disaggregation distribution. (Other alternative possibilities for identification of T_p value are choosing the most dangerous T_p for the considered structure; i.e., equal to the 200%–250% of its first elastic vibration period [5], or considering dependence on event magnitude and computing T_p as function of $M_{p,\mu}$. However, the suggested one seems to be the more rational).
(3) Computing the response spectrum (CIS) as the median of modified GMPE for the $\left\{M_{p,\mu}, R_{p,\mu}, T_{p_\mu}\right\}$ vector. Such a spectrum can be used for the impulsive scenario assuming that modification of ordinary GMPE is sufficient to represent pulse-like characteristics of ground motion or, equivalently, that statistical correlation of spectral ordinates is well accounted for by the GMPE modification factor[IIIII] of Equation (7).
(4) Finally, CIS can be linearly scaled imposing that predicted spectral acceleration is equal to the corresponding hazard value: $S_{a_p}\left(M_{p,\mu}, R_{p,\mu}, T_{p_\mu}\right) = s_a^*$.

6.2. Ordinary (non-pulse-like) scenario

In this case the spectrum has to be representative of the ordinary conditions; therefore, all the available procedure for classical PSHA can be used; e.g., UHS, CMS-ε, etc. That said, for consistency with CIS only, the ordinary spectrum may be defined as (i) computing average values of magnitude and distance from disaggregation distribution given the absence of pulse $f\left(m, r|S_a > s_a^*, NoPulse\right)$ obtaining the vector $\{M_{np,\mu}, R_{np,\mu}\}$; (ii) defining a median spectrum from ordinary GMPE computed with $\{M_{np,\mu}, R_{np,\mu}\}$ values and constant ε; and (iii) scaling the spectrum in a way that predicted spectral acceleration is equal to the hazard value for the period to which disaggregation refers, $S_{a_{np}}\left(M_{np,\mu}, R_{np,\mu}\right) = s_a^*$.

6.3. Design spectra for Application 1

Referring to the hazard result of the SS case with a multiple-magnitude distribution (Sections 4.1 and 5.1), all the mean values of disaggregation distributions necessary to compute discussed design

[IIIII]Discussion of such a hypothesis, while relevant, is out of the scope of this paper.

DOI: 10.1002/eqe

spectra have been computed for three values of spectral periods representative of short (0.5 s), medium (1.0 s), and long (2.0 s) structural periods, as reported in Table I.

In Figure 12 UHS is compared with the two computed spectra defined before for pulse-like, $S_{a_p}\left(M_{p,\mu}, R_{p,\mu}, T_{p_\mu}\right)$, and non-pulse-like, $S_{a_{np}}\left(M_{np,\mu}, R_{np,\mu}\right)$, scenarios. Comparisons are reported in terms of pseudo-accelerations (in logarithmic scale) and displacements (S_d) spectra. It is noted that

Table I. Average disaggregation values for Application 1.

	$M_{p,\mu}$	$R_{p,\mu}$	T_{p_μ}	$M_{np,\mu}$	$R_{np,\mu}$	$P\left(Pulse \mid S_a > s_a^*\right)$	$P\left(NoPulse \mid S_a > s_a^*\right)$
$T=0.5$	5.2	10.9	0.71	5.8	27.9	0.54	0.46
$T=1.0$	5.3	10.5	0.88	5.9	37.0	0.42	0.58
$T=2.0$	5.4	10.2	1.12	6.1	48.7	0.27	0.73

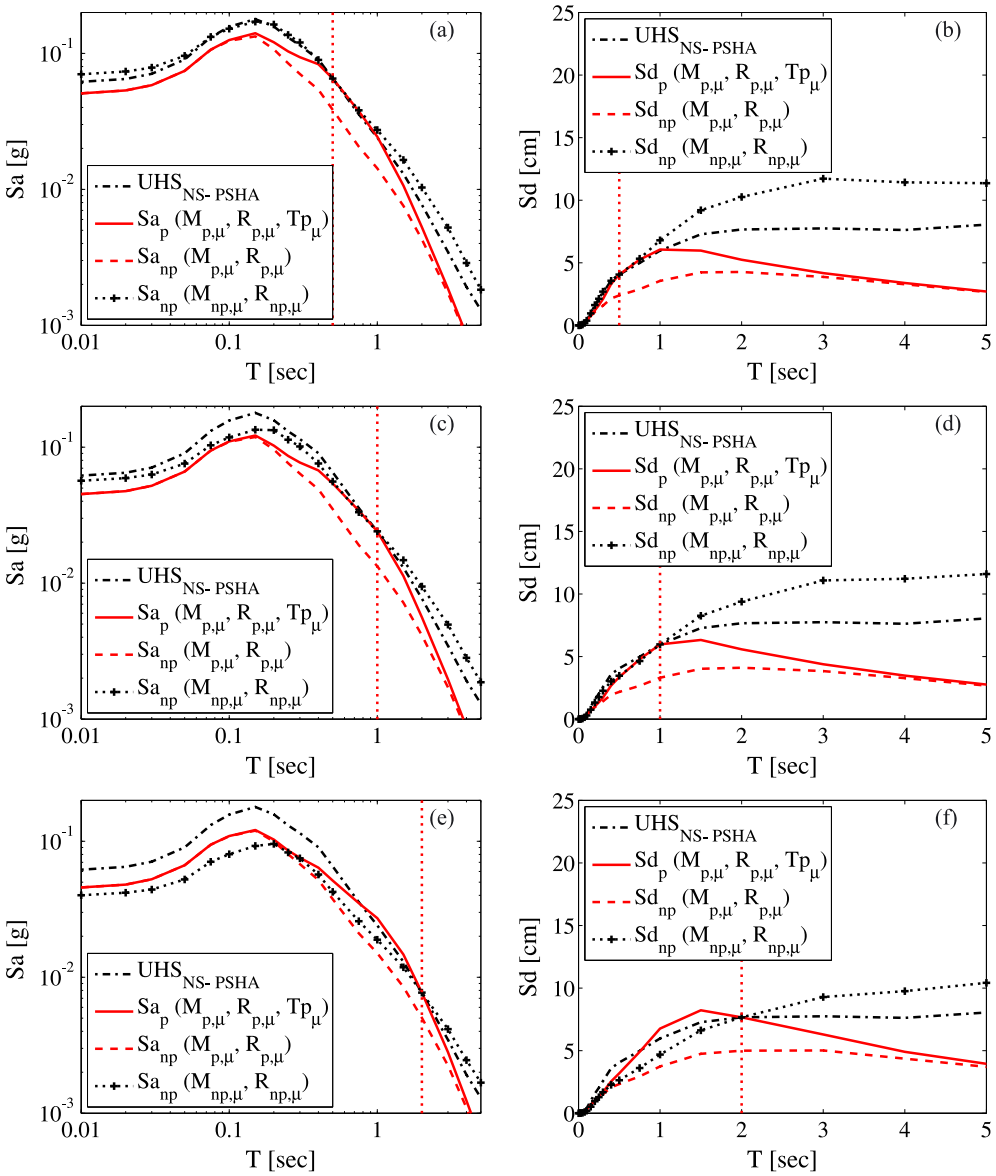

Figure 12. UHS and proposed conditional mean spectra for T equal to 0.5 (a and b); 1.0 (c and d); and 2.0 s (e and f), in terms of accelerations and displacements.

DOI: 10.1002/eqe

S_{a_p} and $S_{a_{np}}$ have significantly different causative magnitude and distance, therefore they are representative of different earthquakes. To underline the characteristic shape of CIS, a spectrum computed from ordinary GMPE with magnitude and distance values of pulse-like scenario $S_{a_{np}}\left(M_{p,\mu}, R_{p,\mu}\right)$, and scaled to the same PGA value of CIS, is also reported in each plot.

Significant ranges of periods are affected by differences between $S_{a_p}\left(M_{p,\mu}, R_{p,\mu}, T_{p_\mu}\right)$ and $S_{a_{np}}\left(M_{p,\mu}, R_{p,\mu}\right)$ spectra, this is because of the shape of modification factor (see also Section 2.3). Moreover, for spectral periods different to the one disaggregation refers to, differences between the proposed spectra and UHS can be significant.

These near-source scenarios may also help in assessing structural performance by means of nonlinear dynamic analysis. In fact, record selection for near-source sites should account for pulse-like and non-pulse-like records. The more straightforward way to address this issue would be to select records with a required M, R, and T_p, from disaggregation. However, because to date it is hard to have ground motion databases with an associated pulse period as metadata, an alternative way can be performing a record selection somehow related to NS spectra. In this framework, marginal pulse occurrence probability from disaggregation and its complementary part, Equation (15), can be used to weigh expected values of structural response (measured by an engineering demand parameter or EDP) for pulse-like (e.g., [30]) and non-pulse-like scenarios, Equation (19).

$$\begin{aligned} E\left[EDP|S_a > s_a^*\right] = {} & E\left[EDP|S_a > s_a^*, Pulse\right]\cdot P\left[Pulse|S_a > s_a^*\right] + \\ & + E\left[EDP|S_a > s_a^*, NoPulse\right]\cdot P\left[NoPulse|S_a > s_a^*\right] \end{aligned} \tag{19}$$

7. CONCLUSIONS

In this paper, the main characteristics of pulse-like ground motions, which are of earthquake engineering interest, were recalled first. These refer to both elastic and nonlinear structural demand. In fact, the main problem is the peculiar spectral shape of pulse-like records, which may cause, depending on the fundamental period of the structure, unexpected (in terms of absolute intensity and with respect to the elastic counterpart) inelastic displacement demands.

Subsequently, starting from the classical PSHA procedure, modifications for near-source conditions able to highlight the ground motion features of interest were analyzed. More specifically, all the models available in literature that allow for the accounting of pulse-like effects in PSHA were reviewed along with the analytical formulation of hazard integrals able to account for them. Considering specific strike–slip and dip–slip fault cases, near-source PSHA was specialized in terms of all the geometrical variables and hypotheses that have to be considered for practical hazard computations.

Modified PSHA procedure was also investigated with respect to disaggregation analysis. This is because identification of probability-based design scenarios and ground motions is even more important, for engineering practice, than seismic hazard itself.

Near-source PSHA was applied to cases of sites subjected to single seismic sources with SS or DS rupture mechanisms, and different magnitude distributions. It was found that the range of spectral periods in which hazard increments, because of forward directivity effects, are structurally significant; shapes of such increments, and periods corresponding to the maximum increment, can be directly derived from the model of magnitude occurrence on the fault. Such a dependency derives from the relationship between pulse period and event magnitude. Thus, if earthquakes are generated with a Gutenberg–Richter relationship, lower structural periods are those most influenced by directivity effects, because of the higher recurrence frequency of smaller magnitudes.

The amount of hazard increments seems to be largely dependent on the characteristics of the studied cases (geometry above all). For those cases studies, variations between 25% and 100% were found with respect to ordinary PSHA. Because the pulse period prediction model depends on the event

DOI: 10.1002/eqe

magnitude with a significant heterogeneity, it was also shown that hazard increments often affect a large range of periods.

Finally, design scenarios in near-source conditions were discussed. Known limits of UHS were found of larger importance in near-source conditions with respect to ordinary PSHA, and a procedure was explored based on NS hazard disaggregation. A close-impulsive spectrum was preliminarily discussed for the pulse-like hazard part, to complement an ordinary spectrum for the non-pulse-like case. These attempts may be helpful in the research for the identification of engineering ground motion characteristics at near-source sites.

ACKNOWLEDGEMENTS

The study presented in this paper was developed within the activities of *Rete dei Laboratori Universitari di Ingegneria Sismica* (ReLUIS) for the research program funded by the *Dipartimento della Protezione Civile* (2010–2013). Authors want to thank the anonymous reviewers for their comments, which improved quality and readability of the paper, and Racquel K. Hagen, of Stanford University, for proofreading the manuscript.

REFERENCES

1. Cornell CA. Engineering seismic risk analysis. *Bulletin of the Seismological Society of America* 1968; **58**:1583–1606.
2. McGuire RK. Seismic hazard and risk analysis. *Earthquake Engineering Research Institute* 2004; MNO-10, 240 p.
3. Somerville PG, Smith NF, Graves RW, Abrahamson NA. Modification of empirical strong motion attenuation relations to include the amplitude and duration effect of rupture directivity. *Seismological Research Letters* 1997; **68**(1):199–222.
4. Baker JW. Quantitative classification of near-fault ground motions using wavelet analysis. *Bulletin of the Seismological Society of America* 2007; **97**(5):1486–1501.
5. Chioccarelli E, Iervolino I. Near-source seismic demand and pulse-like records: a discussion for L'Aquila earthquake. *Earthquake Engineering and Structural Dynamics* 2010; **39**(9):1039–1062.
6. Iervolino I, Chioccarelli E, Baltzopoulos G. Inelastic displacement ratio of near-source pulse-like ground motions. *Earthquake Engineering and Structural Dynamics* 2012. DOI: 10.1002/eqe.2167.
7. Ruiz-Garcìa J. Inelastic displacement ratios for seismic assessment of structures subjected to forward-directivity near-fault ground motions. *Journal of Earthquake Engineering* 2011; **15**(3):449–468.
8. Shahi S, Baker JW. An empirically calibrated framework for including the effects of near-fault directivity in probabilistic seismic hazard analysis. *Bulletin of the Seismological Society of America* 2011; **101**(2):742–755.
9. Abrahamson NA. Effects of rupture directivity on probabilistic seismic hazard analysis. *Sixth international conference on seismic zonation*, 2000.
10. Tothong P, Cornell CA, Baker JW. Explicit directivity-pulse inclusion in probabilistic seismic hazard analysis. *Earthquake Spectra* 2007; **23**(4):867–891.
11. Iervolino I, Cornell CA. Probability of occurrence of velocity pulses in near-source ground motions. *Bulletin of the Seismological Society of America* 2008; **98**(5):2262–2277.
12. Chioccarelli E. Design Earthquakes for PBEE in far-field and near-source conditions. *Ph.D. Thesis*, Dipartimento di ingegneria Strutturale, Università degli Studi di Napoli Federico II, Italy, 2010. Advisors: Manfredi G and Iervolino I. Available at: http://www.dist.unina.it/doc/tesidott/PhD2010.Chioccarelli.pdf
13. Bray JD, Rodriguez-Marek A. Characterization of forward-directivity ground motions in the near-fault region. *Soil Dynamics and Earthquake Engineering* 2004; **24**(11):815–828.
14. Somerville PG. Magnitude scaling of the near fault rupture directivity pulse. *Physics of the Earth and Planetary Interiors* 2003; **137**:201–212.
15. Somerville PG. Development of an improved representation of near fault ground motions. *Proceeding of SMIP98 seminar on utilization of Strong Motion Data, Oakland, CA*, 1998; 1–20.
16. Mavroeidis GP, Papageorgiou AS. A mathematical representation of near-fault ground motions. *Bulletin of the Seismological Society of America* 2003; **93**(3):1099–1131.
17. Alavi B, Krawinkler H. Behavior of moment-resting frame structures subjected to near-fault ground motions. *Earthquake Engineering and Structural Dynamics* 2004; **33**(6):687–706.
18. Tang Y, Zhang J. Response spectrum-oriented pulse identification and magnitude scaling of forward directivity pulses in near-fault ground motions. *Soil Dynamics and Earthquake Engineering* 2010. DOI: 10.1016.
19. Shahi S, Baker JW. Regression models for predicting the probability of near-fault earthquake ground motion pulses, and their period. *Proceeding of 11th International conference on applications of statistics and probability in civil engineering*, Zurich, Switzerland, 2011.
20. Rodriguez-Marek A, Bray JD. Seismic site response for near-fault forward directivity ground motions. *Journal of Geotechnical and Geoenvironmental Engineering* 2006; **132**(12):1611–1620.
21. Baker JW. Identification of near-fault velocity and prediction of resulting response spectra. *Proceeding of Geotechnical Earthquake Engn. Struct. Dyn. IV*, Sacramento, CA, 2008.

22. Boore DM, Atkinson GM. Ground-motion prediction equations for the average horizontal component of PGA, PGV and 5%-damped PSA at spectral period between 0.01 s and 10.0 s. *Earthquake Spectra* 2008; **24**(1):99–138.
23. Wells DL, Coppersmith KJ. New empirical relationships among magnitude, rupture length, rupture width, rupture area, and surface displacement. *Bulletin of the Seismological Society of America* 1994; **87**(4):974–1002.
24. Joyner WB, Boore DM. Peak horizontal acceleration and velocity from strong-motion records including records from the 1979 Imperial Valley, California, earthquake. *Bulletin of the Seismological Society of America* 1981; **71**:2011–2038.
25. Gutenberg B, Richter CF. Frequency of Earthquakes in California. *Bulletin of the Seismological Society of America* 1944; **34**:185–188.
26. McGuire RK. Probabilistic seismic hazard analysis and design earthquakes: closing the loop. *Bulletin of the Seismological Society of America* 1995; **85**:1275–1284.
27. Bazzurro P, Cornell CA. Disaggregation of seismic hazard. *Bulletin of the Seismological Society of America* 1999; **89**:501–520.
28. Iervolino I, Chioccarelli E, Convertito V. Engineering design earthquakes from multimodal hazard disaggregation. *Soil Dynamics and Earthquake Engineering* 2011; **31**(9):1212–1231.
29. Baker JW, Cornell CA. Spectral shape, epsilon and record selection. *Earthquake Engineering and Structural Dynamics* 2006; **35**(9):1077–1095.
30. Sehhati R, Rodriguez-Marek A, El Gawady M, Cofer WF. Effects of near-fault ground motions and equivalent pulses on multi-story structures. *Engineering Structures* 2011; **33**:767–779.

DOI: 10.1002/eqe